A PARAMETRIC STUDY OF THE MOMENTUM FLUX AT THE AIR-SEA INTERFACE

by

Steven J. Lowe

Thesis submitted to the faculty of the
Virginia Polytechnic Institute and State University
in partial fulfillment of the requirements for the degree of

MASTER OF SCIENCE

in

Aerospace Engineering

APPROVED:

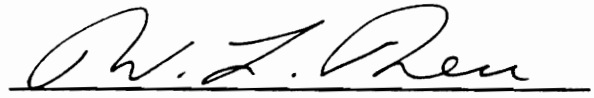

Dr. Wayne L. Neu, Chairman

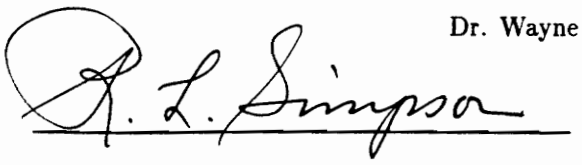

Dr. R. L. Simpson

Dr. W. J. Devenport

February, 1993

Blacksburg, Virginia

A PARAMETRIC STUDY OF THE MOMENTUM FLUX AT THE AIR-SEA INTERFACE

by

Steven J. Lowe

Committee Chairman: Dr. Wayne L. Neu

Aerospace Engineering

(ABSTRACT)

A modified eddy correlation technique is applied to data obtained from a field experiment conducted in the Bight of Abaco during the Spring of 1990. The experiment yielded 3408 30 minute records of turbulent wind data sampled at 5 Hz. Wind stress estimates were successfully calculated for 3182 of these. The modification to the eddy correlation technique involved extending the cospectra to higher frequencies than were measured by the propeller anemometer to obtain a better estimate to the uw covariance. This resulted in a small increase to the uw covariance, and hence the drag coefficient. The regression line fit to the drag coefficients took the form $10^3 C_D = 6.21/\overline{u}_{10} - 0.986 + 0.148 * \overline{u}_{10}$. The data from this experiment clearly indicates a rise in the drag coefficient at lower wind speeds. A turbulent mixing length formulation is presented which sets the foundation for a model to predict the drag coefficient dependence on surface conditions. This formulation predicts a velocity profile which departs from the conventional logarithmic profile near the surface. The mixing length model described here provides a mechanism to relate the scatter in the C_D plots to a wall mixing length. The development of a relation between this wall mixing length and some physical surface wave parameter is left for future work, once the wave data from the experiment becomes available.

ACKNOWLEDGEMENTS

The author wishes to sincerely thank Dr. Wayne L. Neu for his constant encouragement and guidance leading to the completion of this thesis. In addition, the author wishes to thank Dr. Neu for introducing him to the field of atmospheric science. The author also wishes to thank Dr. R. L. Simpson and Dr. W. J. Devenport for serving on his committee and for their criticism of this thesis. The author would like to thank all of his friends in Blacksburg and beyond who have provided help and, when necessary, entertainment throughout his stay at Virginia Tech. The author wishes to especially thank Karen Talley for her love and understanding. Finally, the author would like to acknowledge the constant encouragement and support from his parents, which they have provided throughout his education.

TABLE OF CONTENTS

NOMENCLATURE

B_1	Drag characterization function
C_D	Drag coefficient
$C_{uw}(f)$	u, w cospectral estimate at frequency, f
f	Frequency
f_0	Cutoff frequency within the inertial subrange
$\hat{i}, \hat{j}, \hat{k}$	Unit vectors in x, y, z coordinate directions
L	Monin-Obukov stability scaling parameter
$S(f)$	Autospectral estimate at frequency, f
u	Streamwise component of instantaneous velocity
v	cross flow component of instantaneous velocity
w	Normal component of instantaneous velocity
$\overline{u}$	Streamwise component of mean velocity
$\overline{v}$	cross flow component of mean velocity
$\overline{w}$	Normal component of mean velocity
u'	Streamwise component of fluctuating velocity
v'	cross flow component of fluctuating velocity
w'	Normal component of fluctuating velocity
$\overline{u}_{10}$	Magnitude of velocity vector at 10 m height
u_*	Friction velocity
x	Streamwise position coordinate

y	Cross flow position coordinate
z	Vertical position coordinate
z_o	Roughness length
α	Coefficient to control line placement in the inertial subrange
Δz	Represents wall shift in Rotta 2 model
ϵ	Dissipation rate
κ	Von karman constant; taken to be 0.4
λ_v	Van Driest factor
$\lambda_{v,s}$	Van Driest factor for smooth surfaces
ν	Kinematic viscosity
ϕ_e	Stratification correction function
ρ	Density
τ	Total shear stress at any point in the flow
τ_l	Shear stress due to laminar flow
τ_t	Shear stress due to turbulent flow
τ_w	Total shear stress on the wall
$+$	Superscript denoting a non-dimensional quantity

LIST OF FIGURES

Chapter 1

Introduction

The turbulent momentum flux at the air-sea interface is of utmost importance to the marine environment. The downward momentum flux, (or wind stress), enters the sea surface creating surface waves, surface currents, and turbulence on both sides of the interface. In addition, atmospheric and oceanic circulation models depend on the spatial variability of the wind stress.

The physical problem of evaluating the wind stress is complicated by the interdependence between the wind stress and the waves it creates. Wave-induced pressure fluctuations in the wind field can modulate the local wind shear. In addition, breaking waves increase the momentum flux through turbulent entrainment. The common approach to the problem is to ignore the microscale processes and assume a homogeneous surface which is characterized by a single dominant wave.

Instantaneous wind stress measurements are not easily obtained directly. Therefore, a bulk aerodynamic approach is usually employed which relates the wind stress to the square of the mean wind speed as $\tau = \rho C_D \overline{u}^2$, where ρ is the density and C_D is a drag coefficient. The wind speed must be statistically averaged over sufficiently long temporal scales to eliminate the microscale stress dependencies. Typically C_D is

reported in place of the actual wind stress.

The drag coefficient depends on measurement height, atmospheric stratification, and wave surface conditions. As a convention, C_D data are presented based on a measurement height of 10 m and neutral stratification. Corrections to data taken in non-neutral conditions are readily obtained from heat flux information. However, there is no generally accepted procedure for removing wave surface dependencies. Numerous studies, (e.g. Donelan (1982) and Hsu (1974)), have concluded qualitatively that C_D depends on such parameters as wave slope or fetch but, as of yet, no satisfactory quantitative model exists. It is the intention of the present study to set forth the foundations of a more general and physically sound model than has been attempted in the past.

1.1 Background

1.1.1 The Planetary Boundary Layer, (PBL)

The winds blowing over the Earth's surface form a boundary layer which is quite similar to those studied in the laboratory, with the exception that the PBL is on a much larger scale. Whereas a typical lab boundary layer is on the order of 1 cm, the PBL can extend as high as $1-2$ km. The surface layer is generally considered to be the lowest 10% of the PBL. Within this layer, the variation of momentum flux with height is essentially negligible compared to the mean wind speed gradient. Under very stable conditions, the PBL can be as low as 100 m, but even in this extreme condition our study will take place completely within the surface layer as our measurements are made nominally 8.2 m above the surface.

The effects of surface roughness become quite complex for the PBL. Over land, the roughness can generally be characterized by the dominant feature of the local terrain. This is analogous to the sand-grain roughness scale used by aerodynamicists,

and the familiar shift of the logarithmic velocity profile due to this roughness is seen for the PBL. However, over the ocean, the roughness is not so easily quantified. The local terrain is constantly changing and roughness elements are convecting with the dominant waves. Away from the surface, the net result is still simply a shift of the logarithmic velocity profile. Close to the surface though, it has been shown, (e.g. Takeda 1963) that departures from the logarithmic profile result.

1.1.2 Wind Stress Measurement Techniques

1. *The Profile Method*

   This method is the simplest both conceptually and in implementation, making it the popular choice of experimentalists prior to 1970. The technique is to make velocity measurements at multiple heights and then use the data to find the constants in the logarithmic profile

$$\overline{u} = \frac{u_*}{\kappa}\left\{\log\frac{z}{z_o} - \psi\right\} \tag{1.1}$$

   where z is the measurement height, z_o is a roughness length, κ is the Von karman constant, u_* is the friction velocity defined by $u_*^2 = \tau/\rho$, and ψ is a stability correction function.

   For neutral conditions, $\psi = 0.$, and the above equation can be written in the form

$$\overline{u} = \frac{u_*}{\kappa}\log z - \frac{u_*}{\kappa}\log z_o \tag{1.2}$$

   Then, a plot of $\overline{u}$ vs $\log z$ yields estimates to the wind stress and roughness length through the slope and z-intercept respectively. For non-neutral conditions, the function ψ complicates the above splitting of the logarithmic profile. For this reason, neutral conditions are usually assumed for the use of this method. As is expected, this method works quite well for neutral conditions, but degrades as the stability departs from neutral.

A second limitation to the profile method is the assumption of a logarithmic velocity profile. While this is certainly valid away from the surface, the wave motions on the surface cause departures from the logarithmic profile close to the surface. This requires that all measurements taken for use in the profile method be made sufficiently far away from the surface. Geernaert (1990) suggests that all measurements be made at least three wave heights away from the surface.

2. *The Eddy Correlation Technique*

The eddy correlation technique is widely considered to be the most accurate method of determining the wind stress. In theory, the stress vector is equal to the covariance between the fluctuating vertical and horizontal velocities; or in component form,

$$\vec{\tau} = -\rho \left(\overline{u'w'}\ \hat{i} + \overline{v'w'}\ \hat{j} \right) \tag{1.3}$$

where u is the streamwise velocity, v is the lateral velocity, and w is the vertical velocity. Since the cospectra for wind stress indicate that most of the contributions are from frequencies below 1 Hz, the measurements can be made from propeller anemometers.

The main disadvantage to this method is that the measurements must be made from a stable platform free of any oscillations that could effect the data. An additional concern is that the structure required to keep the instrument stable could cause significant flow distortions.

3. *The Dissipation Technique*

The dissipation technique has become popular because measurements can be made from moving platforms, i.e., ships or buoys. The technique requires only high frequency measurements, (usually by a hot film anemometer), and is therefore unaffected by the low frequency motions of a ship or buoy. The stress

estimate is obtained through the turbulent kinetic energy equation. For neutral or unstable stratifications and steady conditions, this can be written as

$$u_*^3 = \frac{\kappa z \epsilon}{\phi_e} \tag{1.4}$$

where ϵ is the dissipation rate and ϕ_e is a correction function for diabatic conditions. In the inertial subrange, ϵ is related to the wind speed variance spectrum as

$$S(f) = 0.024\epsilon^{2/3}\left(\frac{f}{\overline{u}}\right)^{-5/3} \tag{1.5}$$

The dissipation method provides results in close agreement to the eddy correlation technique for near-neutral conditions. However, Geernaert (1988a) has shown that this method significantly underestimates the magnitude of the stress for stable flow. A more detailed description of the dissipation method is found in Large (1979) and Fairall and Larsen (1986).

1.2 Scope of the Present Study

There are really two phases to the work presented in this paper. First, the process of evaluating the field experiment data is discussed. The primary result of that process is a scatter diagram of drag coefficients as a function of the mean wind speed at 10 m and a regression line representative of that data. The second phase of the study develops the foundation for a model of the drag coefficient dependence on the sea surface conditions.

The calculation of wind stress estimates is achieved via the eddy correlation technique described above. As is usually done, the wind stress vector was assumed to be aligned with the mean wind vector, allowing us to neglect the $\overline{v'w'}$ term. The validity of this assumption will be examined. In addition, a modification was made to the standard eddy correlation technique which extends the uw cospectra to higher

frequencies then were measured. This provides a more accurate calculation of $\overline{u'w'}$. This correction will be discussed in more detail in chapter 3.

The model used to investigate the drag coefficient dependence on sea surface conditions involves the use of turbulent mixing length theory. It is proposed that a non-zero wall mixing length provides a mechanism to model the sea surface dependence. There are two reasons for the use of mixing lengths. First, the velocity profile obtained from mixing length formulations predicts a departure from the logarithmic profile close to the surface. This is in accordance with what has been observed for the PBL over the ocean. Second, a previous study has shown that a mixing length model predicts a rise in drag coefficients at lower wind speeds, (e.g. Balachandran, 1986). This trend is clearly indicated by the data presented in this paper.

Chapter 2

The Data Set

The data used for this research was obtained from a field experiment conducted during the Spring of 1990. The experiment took place in the Bight of Abaco; a 100 km by 40 km section of the Little Bahama Bank. The bight is unique in that it is almost completely enclosed by either land or shallow sand bars so that virtually all wave energy in the bight is generated within the bight. The experiment was repeated in the Spring of 1991, but this data is still being analyzed and is therefore not included in this paper. This work was sponsored by the National Science Foundation as part of a larger program studying the evolution of the surface wave spectrum (see Snyder et al., 1990).

2.1 The experiment

The turbulent wind fluctuations were measured using K-Gill propeller vane anemometers mounted atop weather stations. Figure 2.1 is a sketch of one such weather station. Note that the anemometer is mounted on a guyed 1 inch pole so that it is virtually free of flow distortions. The measurement height of the anemometer is nominally 8.2 m. Each weather station was also equipped with a tide gauge and, for 1991 only, air and sea temperature gauges. The spatial distribution of the weather

stations for the 1990 experiment is shown in Figure 2.2.

The instruments were operated remotely via a radio link to the base station. Upon instruction, each instrument performed "high speed" data collection for 30 minutes at a 5 Hz sample rate, storing the data on board until it was instructed to telemeter the data to the base station. High speed data consisted of the voltage outputs from the wind vane and two propeller signals. All three signals were low-pass filtered prior to sampling using a four pole Bessel filter with a cutoff frequency of 2 Hz.

Each station also collected "low speed" data continuously, (except during data telemetry), at a sample rate of 0.25 Hz. This data consisted of the same three signals as the high speed data plus tide gauge readings and, for 1991, temperature gauge readings. Air and sea temperature measurements were made at the base camp in 1990. The tide gauge readings were intended to provide accurate anemometer elevations for use in the drag coefficient calculations. However, since the measured tidal range was always within $\pm$ 0.3 m, the effect of elevation changes on the drag coefficients is negligible.

For the 1990 experiment, only stations 11-14 were operable. Stations 11 and 12 yielded one high speed record per hour. Stations 13 and 14 provided two records per hour which implies essentially continuous data. We have a total of 3408 records from this experiment. Figure 2.3 shows one hour averages of wind speed and direction at station 13.

During the 1991 experiment, all five stations were used. Due to the increased data flow, the sampling rate was reduced to 4 Hz. In addition, only station 14 gave two high speed records per hour. This led to 3621 records for the 1991 experiment. Humidity measurements were made at the base station to supplement the air and sea temperature readings added to the low speed data.

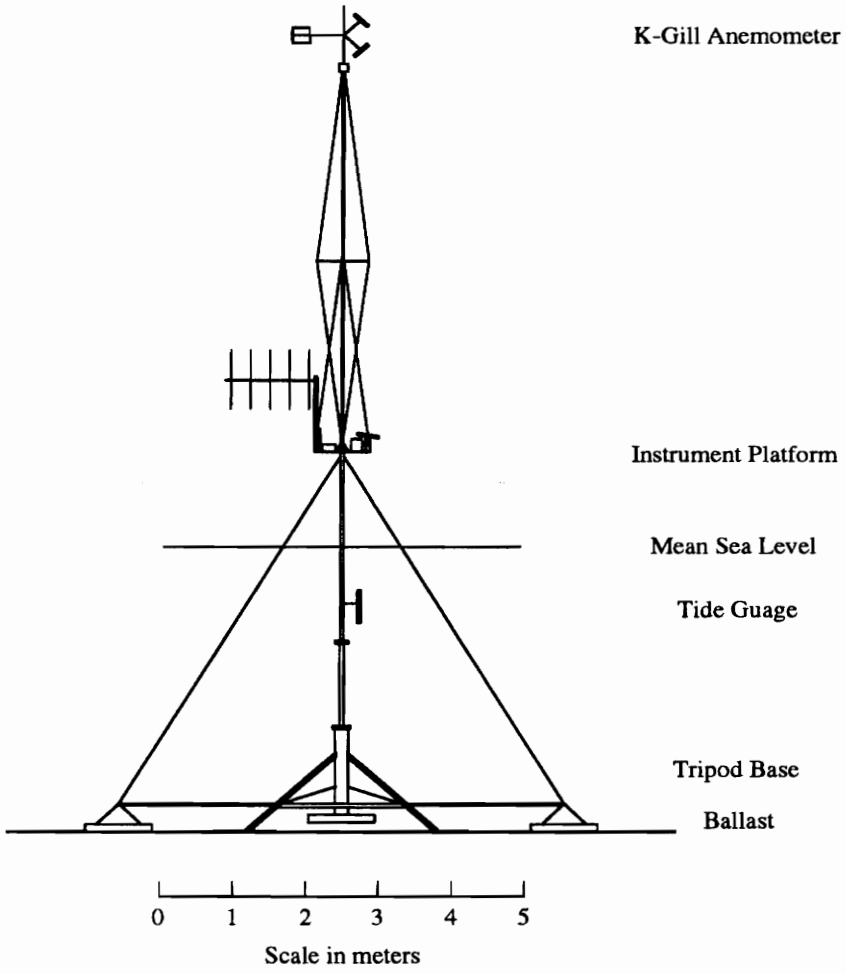

Figure 2.1: Weather Station sketch. Not shown are air and water temperature transducers added for the 1991 experiment.

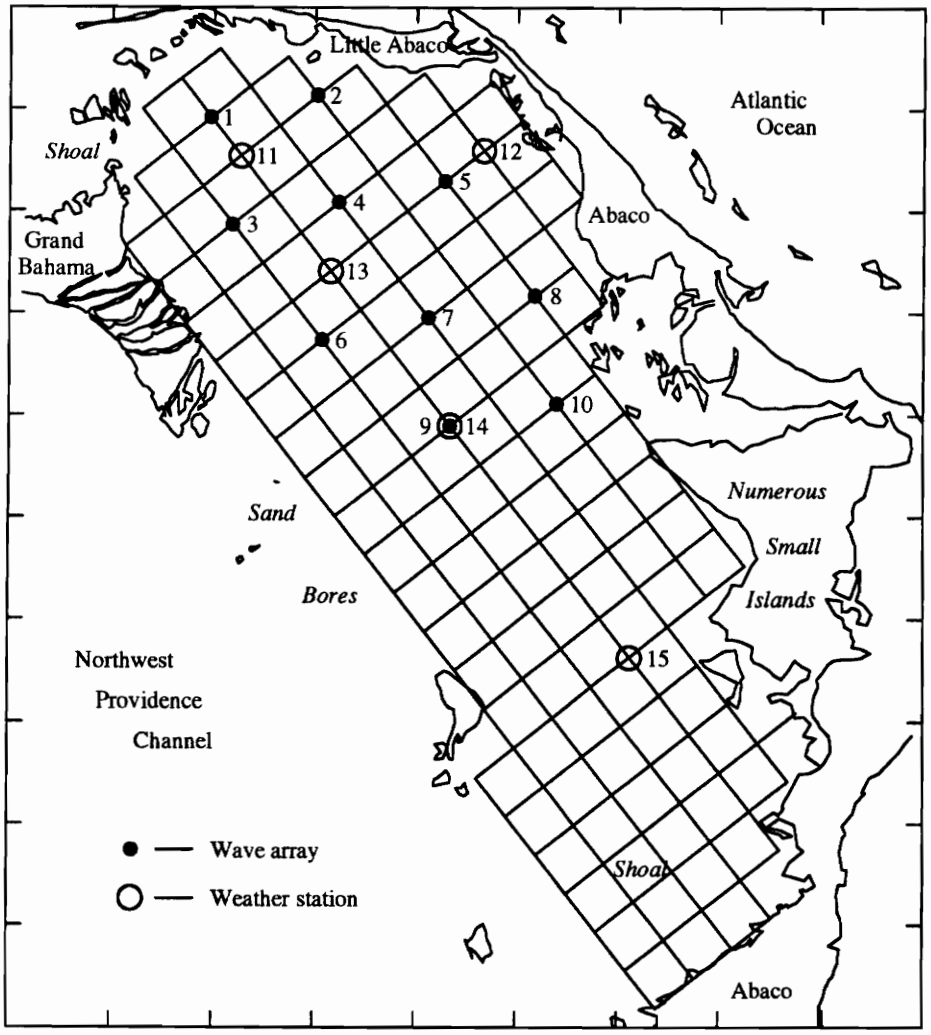

Figure 2.2: Station locations for the spring 1990 field experiments. Grid is 4.8×4.8 km; border scale is 10 km per division. Also shown are the wave array locations.

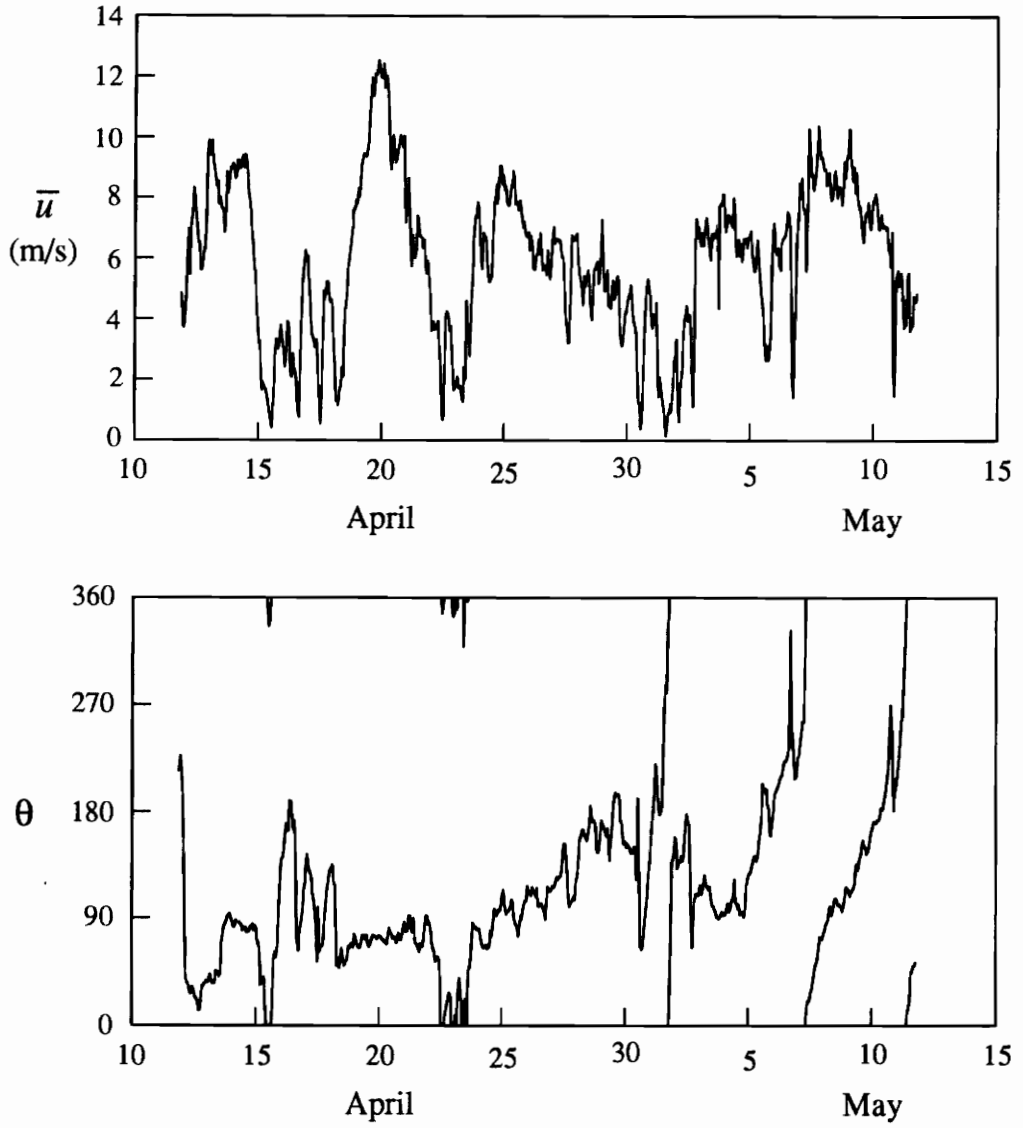

Figure 2.3: One hour averages of wind speed and direction at station 13 during the 1990 field experiment. Wind direction is direction from which wind is blowing in degrees clockwise from north.

2.2 Data Analysis

In this section, the first stages of analysis done to the 1990 data is discussed. This includes the translation of data into physical variables and the calculation of cospectra. The use of this data, as it pertains to the calculation of wind stress estimates, is contained in chapter 3.

2.2.1 Data Translation

Instantaneous values of the wind direction, elevation angle, and magnitude were calculated from the recorded output levels of the wind vane and two propeller signals contained in the high speed data files. The wind direction indicates the direction from which the wind was blowing, measured clockwise from north. The wind magnitude and elevation angle were obtained using the table lookup scheme developed by Wei (1990).

The instantaneous wind vectors were averaged over the entire record and then transformed to a new coordinate system defined by the mean wind vector. The transformed vectors were expressed in a cartesian coordinate system defined by $\vec{U} = (u, v, w)$, where u is along the mean wind vector, v is in the horizontal cross flow direction, and w completes the right hand system. Each component was then broken into mean and fluctuating parts

$$\begin{aligned} u &= \overline{u} + u' \\ v &= \overline{v} + v' \\ w &= \overline{w} + w' \end{aligned} \tag{2.1}$$

where the mean quantities $(\overline{u}, \overline{v}, \overline{w})$ are defined as averages over the 30 minute record.

The converted data was stored in files containing the mean quantities on the first line followed by only the fluctuating part of each instantaneous wind vector. A

statistical summary file was created for each station giving the mean wind speed, direction, and elevation angle, the u', v', and w' variances, and the u', w' and v', w' correlations.

During data translation, the wind vane signal was continually monitored for what we called "the gap error". The potentiometers used to indicate the wind vane direction were supposed to have a 5° dead band between the zero and full scale voltage positions. In actuality, if the mean wind direction fell within this 5° band, the potentiometer recorded swings of 355°, resulting in large variances and a bad wind direction measurement. These sections of data were detected, counted, and corrected whenever possible. However, if a major portion of a record was characterized by this error, it had to be discarded.

2.2.2 Cospectrum Calculation

The uw cross-spectrum, (using the u' and w' fluctuations about a 30 minute mean as defined above), was calculated for each data record using the PERIODOGRAM algorithm in Marple (1987). A Hamming window was employed with 80 samples per segment and 50% overlap. Using zero padding, 128 evenly spaced estimates were obtained from zero up to the Nyquist frequency. This implies a frequency increment of $5/256$ Hz for the 1990 data. Note that the u and w autospectra were also produced along with the cospectra.

The calculated spectral estimates had to be adjusted for the frequency response of the anemometer. Wei (1990) compared the simultaneous turbulent wind measurements made with the K-Gill anemometer to those made by a triple hot wire jig. The anemometer was found to be characterized by a single pole filter with a distance constant of 1.34 m. The anemometer manufacturer, R.M. Young Co., claims a distance constant of 1.0 m for the propellers used. However, since the propellers were at an angle of 45° to the mean wind, the effective distance constant is increased. The low-

pass filtering of the anemometer signals before the A/D conversion had a negligible effect on frequencies below 1 Hz, (the effective limit of the instrument's response). Therefore, no correction was applied for the use of this filter.

Chapter 3

Wind Stress Analysis

This chapter discusses the procedure used to obtain wind stress estimates from the calculated cospectra. The results are presented in terms of drag coefficients and the major trends identified. Also included is a short investigation of the wind stress angle relative to the mean wind direction.

3.1 Calculation of Wind Stress

The calculation of shear stresses is accomplished using a modified eddy correlation technique, which states that the shear stress is equal to the covariance of the fluctuating components of the horizontal and vertical wind speeds. If we assume that the surface stress is essentially aligned with the mean wind vector, we can write

$$\frac{\tau}{\rho} = -\overline{u'w'} \tag{3.1}$$

The quantity $\overline{u'w'}$ is obtained from the cospectrum, $C_{uw}(f)$, by

$$\overline{u'w'} = \int_0^\infty C_{uw}(f)df \tag{3.2}$$

However, the propeller anemometer used is unable to resolve high frequency velocity fluctuations due to its limited frequency response. This results in slightly low estimates of the wind stress. To correct for this, the cospectrum was extended into the

inertial subrange using the theoretically known power law, $C_{uw}(f) \propto f^{-7/3}$, (Panofsky, 1984). The integral of equation (3.2) is evaluated up to some cutoff frequency within the inertial subrange using actual data, and analytically solved beyond. This results in

$$\overline{u'w'} = \int_0^{f_0} C_{uw}(f)df + \frac{3}{4} f_0 C_{uw}(f_0) \tag{3.3}$$

Rather than just extend a line $\propto f^{-7/3}$ from f_0, we felt it better to fit the line through the cospectra starting at f_0. This was done by solving for the coefficient α in

$$\int_{f_0}^{f_b} C_{uw}(f)df = \int_{f_0}^{f_b} \alpha f^{-\frac{7}{3}} df = \frac{3}{4}\alpha \left(f_0^{-\frac{4}{3}} - f_b^{-\frac{4}{3}} \right) \tag{3.4}$$

For our study, f_0 was taken as the frequency of the 4^{th} point past the peak in the first moment of the cospectrum and f_b was the minimum of either the frequency of the 29^{th} point past the peak or the frequency of the last point at which a spectral estimate was saved. Once α is obtained, the wind stress estimate becomes

$$u_*^2 = -\overline{u'w'} = -\left\{ \int_0^{f_0} C_{uw}(f)df + \frac{3}{4}\alpha f_0^{-\frac{4}{3}} \right\} \tag{3.5}$$

Figures (3.1) and (3.2) show examples of the calculated cospectra and the power law fit. Figure (3.1) is indicative of cases with a good fit while Figure (3.2) displays a case with very poor fit. The higher wind speed cases ($> 4\ m/s$), generally displayed cleaner cospectra with better fits. In general the correction resulting from this technique was actually quite small. The corrected $\overline{u'w'}$ values were usually less than 5% larger than those obtained from the direct correlation.

In some cases, the cospectra calculation resulted in a positive $\overline{u'w'}$. This leads to a negative drag coefficient so these points were discarded. This error primarily occurred during very low wind speed conditions. Of the original 3408 high speed data files, 226 were discarded leaving 3182 files for which wind stress estimates were successfully calculated. The following section discusses the calculation of drag coefficients for each of these points.

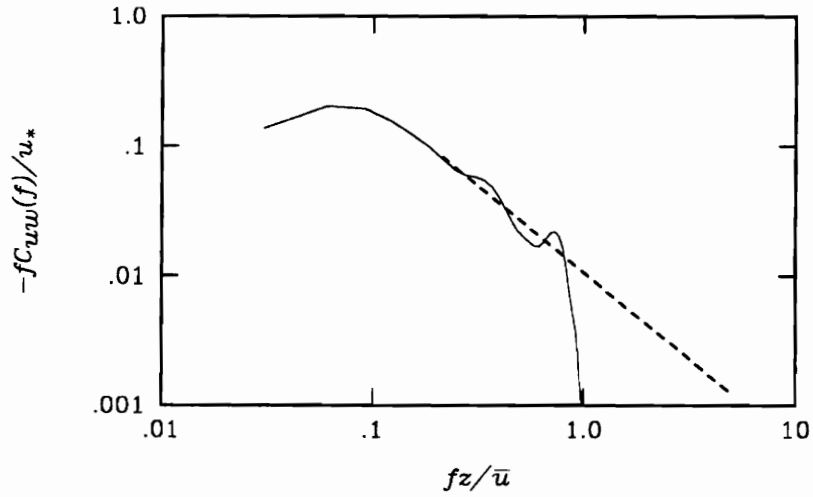

Figure 3.1: Normalized cospectrum (solid line) and its inertial range extension (dashed line). Example of good fit, $\overline{u} = 5.25\ m/s$.

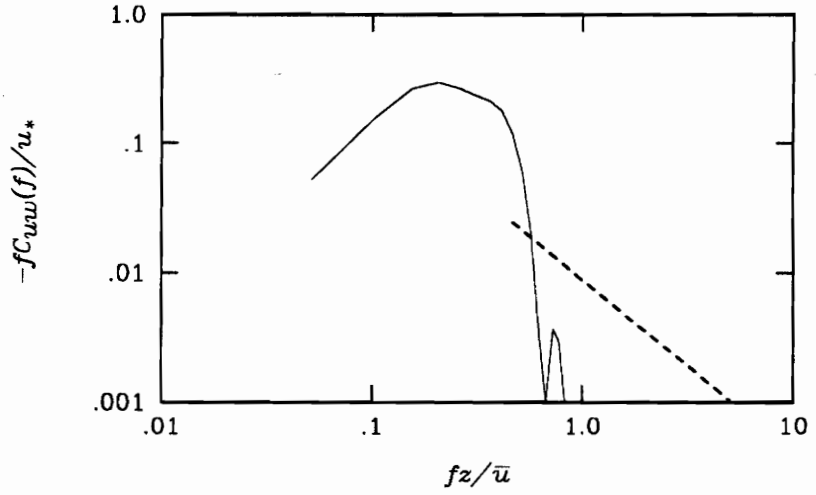

Figure 3.2: Normalized cospectrum (solid line) and its inertial range extension (dashed line). Example of bad fit, $\overline{u} = 3.1\ m/s$.

3.2 Drag Coefficients

It is customary in the study of the air-sea interface to discuss the wind stress in terms of the bulk aerodynamic parameter, C_D, which is defined by the momentum flux equation

$$\tau = \rho \, C_D \overline{u}_{10}^2 \tag{3.6}$$

where $\overline{u}_{10}$ is the mean wind speed at a height of 10 m. Using the definition of the friction velocity, $u_*^2 = \tau/\rho$, and solving for C_D leads to the relation

$$C_D = \left(\frac{u_*}{\overline{u}_{10}}\right)^2 \tag{3.7}$$

where u_*^2 comes from equation (3.5).

The mean wind speed at 10 m is used as a convention. Our measurements at 8.2 m had to be transferred to the 10 m height assuming a logarithmic mean velocity profile as

$$\overline{u}_{10} = \frac{u_*}{\kappa} \log(\frac{10}{8.2}) + \overline{u}_{8.2} \tag{3.8}$$

Note that there is no stability correction in the above relation. Stability estimates would normally come from the difference in air and water temperatures. However, during the 1990 field experiment, air and water temperature measurements were made at the base camp, with the air temperature obtained over land. Figure 3.3 shows a history of the air and water temperatures for 1990. The large swings in the air temperature are due to radiation effects over the land and therefore can not be considered indicative of the air temperature over the water.

Stability estimates made from these data resulted in unrealistically large corrections to the drag coefficients. However, because the actual stability was always near neutral and since we have such a large data set covering all times of day, it is argued that curve fits through our uncorrected data will be very close to curve fits through stability corrected data. Therefore, we will treat the resulting regression lines as neutrally stratified.

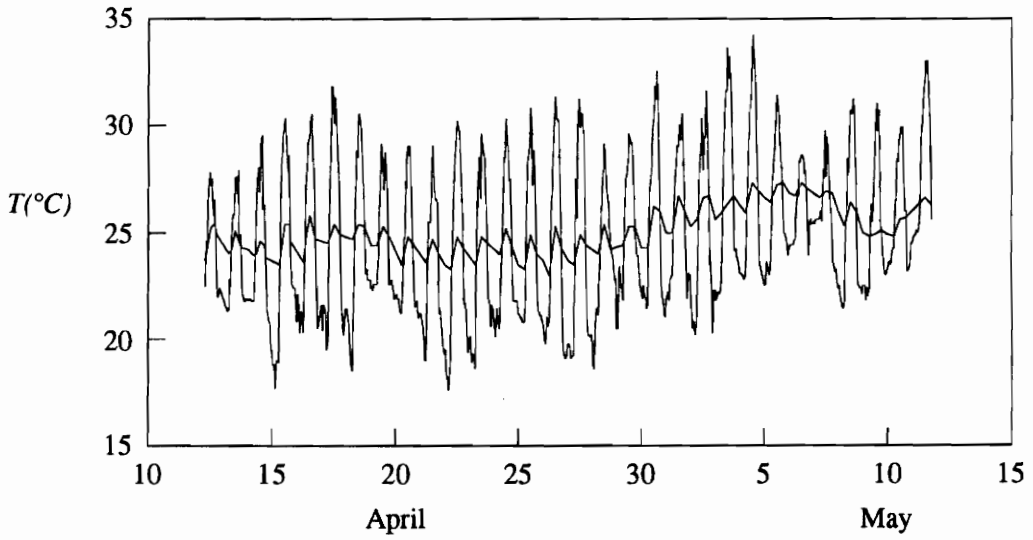

Figure 3.3: Air and water temperatures at the base camp during the 1990 experiment.

During the 1991 experiment, air and water temperature measurements were made at each station. These will be used to apply more accurate stability corrections to the 1991 data. A comparison of the regression line fit to the 1991 stability corrected drag coefficients and the 1990 regression line will provide a basis for evaluating the validity of the above assumption about the 1990 data.

3.2.1 Results

Figure 3.4 is a plot of the drag coefficients for the 1990 data set. A least squares curve fit of the form

$$10^3 C_D = 6.21/\overline{u}_{10} - 0.986 + 0.148\overline{u}_{10} \tag{3.9}$$

is shown through the data. The fit was made over the range $2 \leq \overline{u}_{10} \leq 10\ m/s$ which includes 2898 data points. The RMS error of the fit is 0.389. Also included on the figure is two drag coefficient fits from previous studies by Geernaert et al. (1988b) and the eddy correlation results of Large and Pond (1981). These curves are of the form $10^3 C_D = 5/\overline{u}_{10} + 0.07\overline{u}_{10}$ and $10^3 C_D = 0.46 + 0.069\overline{u}_{10}$ respectively.

The data clearly shows a rise in drag coefficient at the lower wind speeds, which is also supported by the Geernaert curve. A possible explanation lies in the theory that the drag coefficient increases with the slope of the wave surface. At lower wind speeds, the waves are smaller but tend to be steeper; thus the increase in drag. At higher wind speeds, our data approaches the Large and Pond curve. The data above 10 m/s seems to fall below the trend of the rest of the data. These points represent a strong easterly wind which occurred during one short period of the experiment. The reason for these low C_D's is not yet known.

Figure 3.5 displays the same data in an alternate form which helps to quantify the amount of scatter. The data is broken into 0.5 m/s wind speed intervals and each symbol on the plot represents the mean value $\pm$ one standard deviation of the

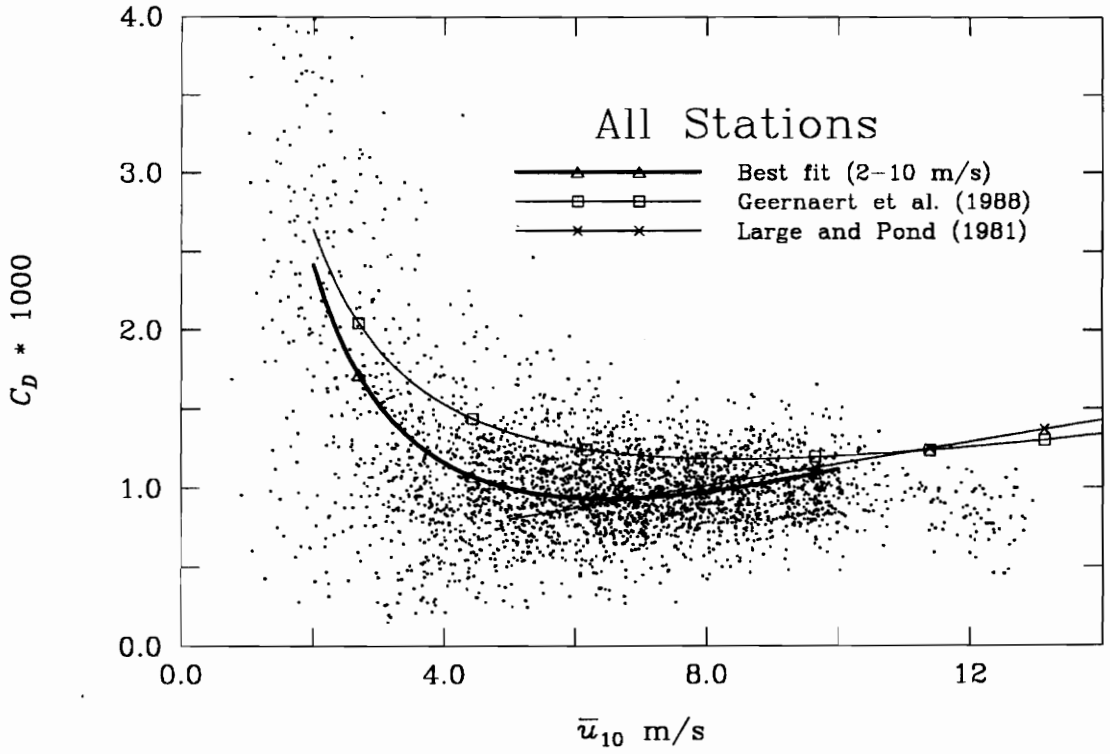

Figure 3.4: Drag coefficients from all stations with best fit to the range $2 - 10\ m/s$. Also shown are the fits from Geernaert et al. (1988b) and the Large and Pond (1981) eddy correlation results.

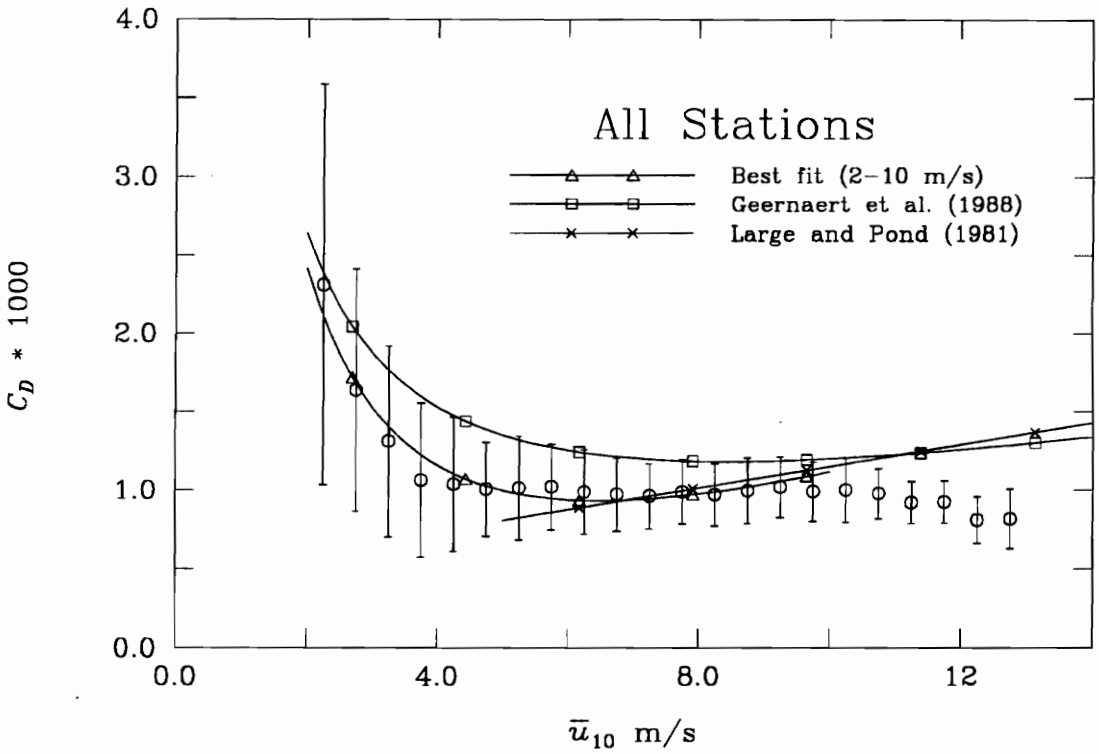

Figure 3.5: Drag coefficient data of Figure 3.4 grouped in 0.5 m/s bands. Symbols represent mean $\pm$ one standard deviation for each band. Also shown are the same fits seen in Figure 3.4

C_D values in that interval. Table 1 displays the same information numerically along with the number of data points in each interval. The large number of points in each interval below 10 m/s implies that statistically significant conclusions can be drawn from the data in any one interval. The scatter in each interval is presumed to be due to varying surface conditions. A model to correlate the scatter to a wall mixing length is presented in Chapter 4.

Table 3.1 : C_D statistics in 0.5 m/s intervals

Wind Speed Range (m/s)	Mean $10^3 C_D$	Number of Records	Standard Deviation
2.0 to 2.5	2.310	79	1.276
2.5 to 3.0	1.638	90	.773
3.0 to 3.5	1.311	124	.607
3.5 to 4.0	1.064	152	.491
4.0 to 4.5	1.038	172	.428
4.5 to 5.0	1.006	195	.299
5.0 to 5.5	1.013	198	.332
5.5 to 6.0	1.021	212	.272
6.0 to 6.5	.989	268	.268
6.5 to 7.0	.973	275	.232
7.0 to 7.5	.961	239	.206
7.5 to 8.0	.989	230	.206
8.0 to 8.5	.971	193	.199
8.5 to 9.0	.996	194	.211
9.0 to 9.5	1.019	151	.193
9.5 to 10.0	.991	126	.190
10.0 to 10.5	1.001	55	.204
10.5 to 11.0	.978	20	.159
11.0 to 11.5	.920	16	.135
11.5 to 12.0	.924	19	.135
12.0 to 12.5	.809	29	.147
12.5 to 13.0	.816	15	.189

3.3 Wind Stress Angles

As was mentioned earlier, the true definition of the wind stress vector is

$$\vec{\tau} = -\rho \left(\overline{u'w'}\ \hat{i} + \overline{v'w'}\ \hat{j} \right)$$

From this a wind stress angle relative to the mean wind direction can be defined as

$$\theta = \tan^{-1} \left(\frac{\overline{v'w'}}{\overline{u'w'}} \right) \tag{3.10}$$

It is clear then that by neglecting the $\overline{v'w'}$ component of the wind stress, one assumes that the stress vector is aligned with the mean wind direction. By plotting the stress vector direction against the mean wind direction, the above assumption can easily be assessed.

This was done for each of the stations and the results for station 14 are shown in Figure 3.6. The stress vector tends to be to the left of the mean wind, but the majority of points are less than 20° off. This implies an error of 6% in the stress estimate. It is interesting to note that the stress vector aligns much better with the mean wind for north to east winds than for east to west winds. A possible explanation for this is that the waves in the Bight are often skewed relative to the mean wind direction due to the elongated shape of the bight and its depth variation. Hopefully, the forthcoming wave data will shed more light on this subject.

In recognition of the fact that the stress often departed significantly from the mean wind direction, the drag coefficients were recalculated using

$$u_*^2 = \left[\overline{u'w'}^2 + \overline{v'w'}^2 \right]^{1/2} \tag{3.11}$$

where the direct correlations were used for $\overline{u'w'}$ and $\overline{v'w'}$. The resulting least squares curve fit over the same range of $2 \leq \overline{u}_{10} \leq 10\ m/s$ took the form $10^3 C_D = 7.43/\overline{u}_{10} - 1.16 + 0.152\overline{u}_{10}$ with an increased RMS error of 0.425. The drag coefficients increased only slightly, ($\sim$ 5%), indicating that on average the assumption used in the eddy correlation technique did not effect the final results.

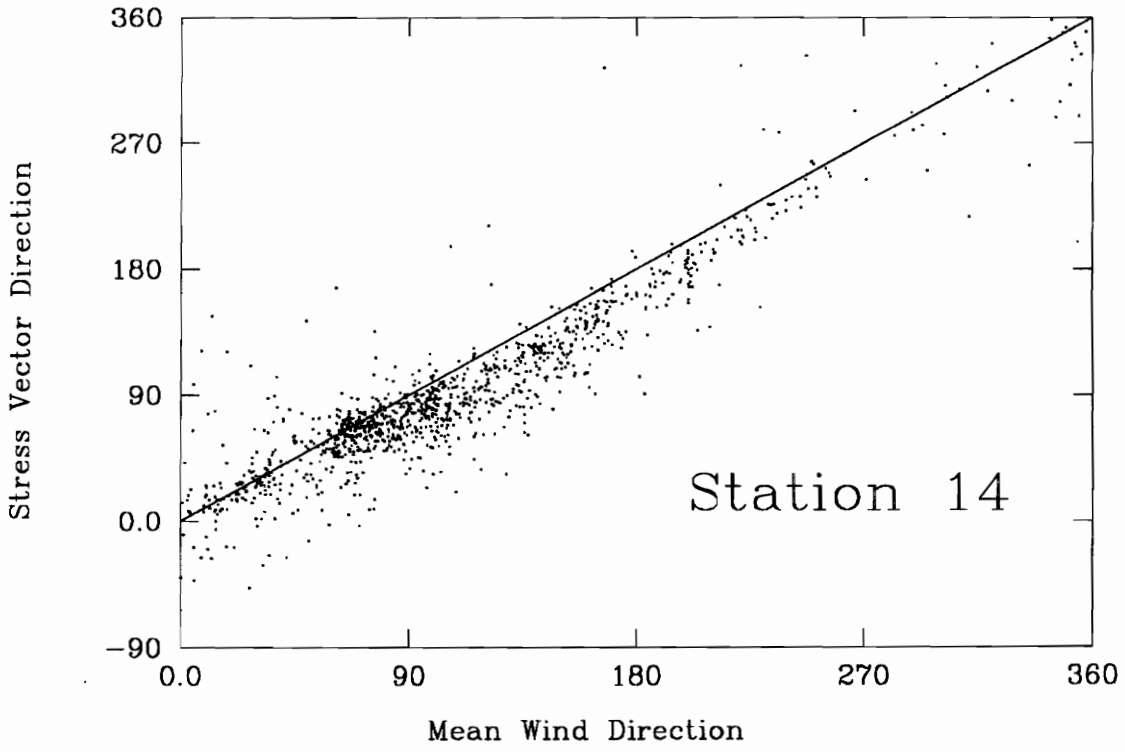

Figure 3.6: Direction of wind stress vector vs. mean wind direction at station 14. Direction indicates direction from which the wind was blowing, measured clockwise from north.

Chapter 4

Mixing Length Models

The scatter in the C_D results of the previous chapter is usually attributed to varying surface conditions. In this section, a mixing length model is developed which provides a mechanism to correlate the scatter in the C_D plots to a mixing length at the wall. Although it is not the purpose of this paper, it is proposed that this wall mixing length parameter can be related to some physical wave surface parameter such as wave slope or age. The determination of such a relation will be the subject of a future study once the wave data from the experiment becomes available.

In developing the mixing length models, a more general form of the logarithmic velocity profile is used,

$$u^+ = \frac{1}{\kappa} \log(z^+) + B_1 \tag{4.1}$$

where $u^+ = u/u^*$, $z^+ = zu^*/\nu$, ν is the kinematic viscosity, and B_1 is considered to be a roughness drag characterization function. B_1 will become very useful for implementing boundary conditions on the mixing length model velocity profiles.

4.1 Mixing Length Theory

The total shear stress τ at any point in a flow is equal to the sum of the laminar, τ_l ,and turbulent, τ_t , shear stresses. Newton's Law of Viscosity models the laminar shear stress as

$$\tau_l = \mu \frac{du}{dz} \tag{4.2}$$

Prandtl (1925) proposed for the turbulent shear stress the so-called mixing length formulation such that

$$\tau_t = \rho \ell^2 \left(\frac{du}{dz}\right)^2 \tag{4.3}$$

where ℓ is the mixing length which is considered to be a function of its position in the flow. Substitution of the two shear stresses results in

$$\frac{\tau}{\rho} = \nu \left(\frac{du}{dz}\right) + \ell^2 \left(\frac{du}{dz}\right)^2 \tag{4.4}$$

For a surface layer with zero longitudinal pressure gradients, τ becomes approximately equal to the wall shear stress, τ_w. With this assumption, $\frac{\tau}{\rho}$ is equal to u_*^2 throughout the region of interest. This allows equation (4.4) to be written in the simple non-dimensional form

$$\ell^{+2} \left(\frac{du^+}{dz^+}\right)^2 + \left(\frac{du^+}{dz^+}\right) = 1 \tag{4.5}$$

where $\ell^+ = \ell u^*/\nu$. Upon solving this quadratic equation for $\frac{du^+}{dz^+}$ and integrating from the wall where $u^+ = 0$ and $z^+ = 0$ to some arbitrary z^+, the mixing length velocity profile is obtained,

$$u^+ = \int_0^{z^+} \frac{2}{1 + \sqrt{1 + (2\ell^+)^2}} dz^+ \tag{4.6}$$

With the proper selection of ℓ^+ the above equation yields a velocity profile which is of logarithmic form for large z^+ but that departs from logarithmic close to the surface. The following section describes various models for ℓ^+ which have been found to achieve this result.

4.2 Models for ℓ^+

Prandtl proposed the simple linear relation

$$\ell^+ = \kappa z^+ \tag{4.7}$$

Substitution of this relation into equation (4.6) results in a completely logarithmic velocity profile. A modification function, M, (to be used as $\ell^+ = M\kappa z^+$), is needed to adjust Prandtl's relation as it nears the wall. For smooth surfaces, Van Driest (1956) proposed

$$M = 1 - \exp(\frac{-z^+}{\lambda_v^+}) \tag{4.8}$$

where λ_v^+ is a nondimensional quantity called the Van Driest factor. Note that M is zero at $z^+ = 0$ and approaches unity as $z^+ \to \infty$ so that Van Driest's model approaches Prandtl's linear model away from the wall. λ_v^+ is supposed to represent a dimensionless effective frequency of turbulent fluctuations. In reality though, it is nothing more than a "fix-it" factor used to obtain a good fit for data in the sublayer and log regions. For this reason, the Van Driest model is generally not accepted by the boundary layer community.

Rotta (1950,1962) developed extensions for rough surfaces to both the Prandtl and Van Driest models. Rotta's first model assumed a laminar sublayer thickness, z_L^+, such that

$$\ell^+ = \kappa(z^+ - z_L^+) \tag{4.9}$$

Substitution of this ℓ^+ into equation (4.6) and integrating results in

$$u^+ = z_L^+ + \frac{1}{\kappa}\left(\log(4\kappa z^+) - 1\right) \tag{4.10}$$

Equating (4.10) with the logarithmic velocity profile, equation (4.1), and noting that z_L^+ tends to zero with increasing roughness results in

$$B_1 = \frac{-1}{\kappa}\left(1 - \log(4\kappa)\right) = -1.325$$

This B_1 is considered to be the bounding value for fully rough flow.

Rotta then assumed the existence of a non-zero mixing length at the wall, ℓ_w^+, to characterize the roughness. Prandtl's model becomes

$$\ell^+ = \ell_w^+ + \kappa z^+ \tag{4.11}$$

Substitution of this model into equation (4.6) results in the modified velocity profile:

$$u^+ = \frac{1}{\kappa l^+}\left(\frac{1}{2} - \sqrt{\ell^{+2} + \frac{1}{4}}\right) - \frac{1}{\kappa l_w^+}\left(\frac{1}{2} - \sqrt{\ell_w^{+2} + \frac{1}{4}}\right) + \frac{1}{\kappa} log\left(\frac{\ell^+ + \sqrt{\ell^{+2} + \frac{1}{4}}}{\ell_w^+ + \sqrt{\ell_w^{+2} + \frac{1}{4}}}\right) \tag{4.12}$$

As $z^+ \rightarrow \infty$ this relation reduces to the logarithmic profile with

$$B_1 = \frac{1}{\kappa}(log 4\kappa - 1) - \frac{1}{\kappa \ell_w^+}\left(\frac{1}{2} - \sqrt{\ell_w^{+2} + \frac{1}{4}}\right) - \frac{1}{\kappa} log\left(2\ell_w^+ + 2\sqrt{\ell_w^{+2} + \frac{1}{4}}\right) \tag{4.13}$$

This implies that for a given set of data, (typically $\overline{u}_{10}$ and u_*), B_1 can be found from equation (4.1) and then l_w^+ is obtained from equation (4.13). Balachandran (1986) successfully demonstrated this scheme for data in the fully rough regime. However, upon implementing this model using our data, it was found that we frequently had flow conditions representative of the intermediate roughness regime, ($-1.325 < B_1 < 5.21$). Figure 4.1 displays the range of B_1 values obtained from equation (4.1) using equation (3.9) for the average C_D values at each wind speed. Unfortunately, this model is only defined for the fully rough regime and so it can not be applied to the full range of our data.

For the purpose of demonstration, the model was applied to the portion of our data in the fully rough regime, ($\overline{u}_{10} \leq 3.6\ m/s$), and to the Geernaert data which is seen to be always within the fully rough regime on Figure 4.1. The resulting distribution of ℓ_w^+ with wind speed is shown in Figure 4.2. This curve corresponds to the expected wall mixing length, or surface condition, for the given wind speed. As is required by Rotta's model, the wall mixing length goes to zero at $\overline{u}_{10} = 3.6\ m/s$, the point at which our data is no longer fully rough.

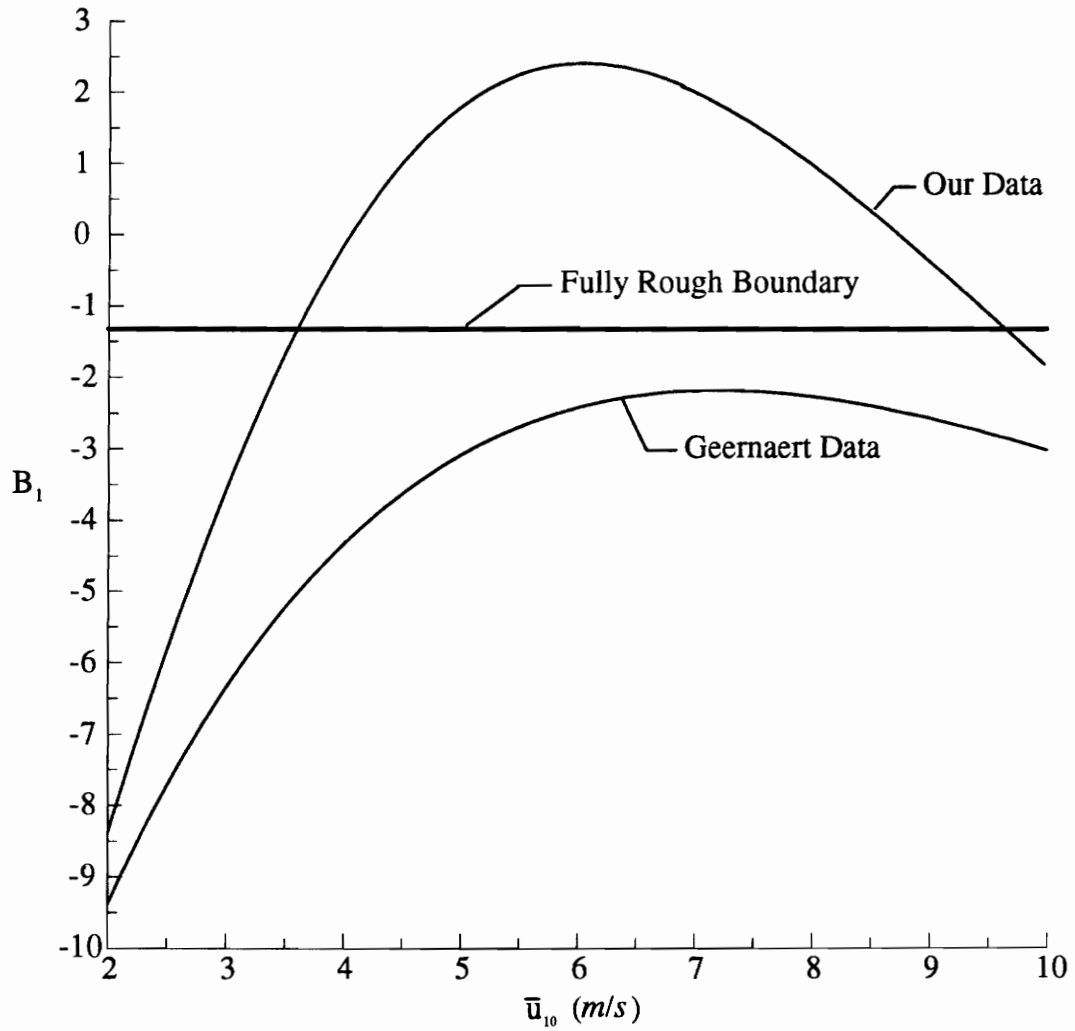

Figure 4.1: Range of B_1 using the C_D regression line through our data and the Geernaert, (1987), curve. Also shown is the boundary for the fully rough regime.

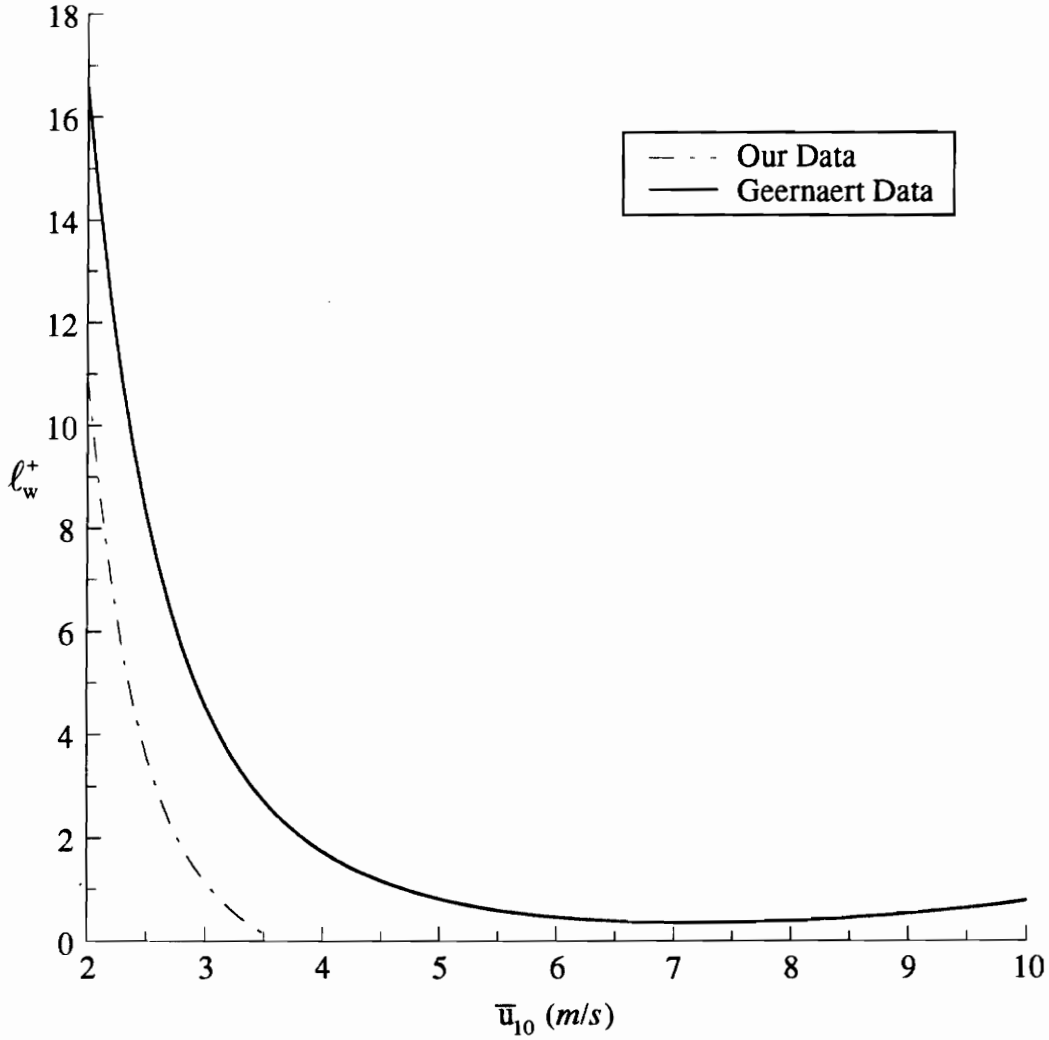

Figure 4.2: Expected wall mixing length for a given mean wind speed using the Rotta 1 model and the same C_D regression lines as in Figure 4.1.

Rotta's second model, (which will be referred to as Rotta 2), provides a similar relation between B_1 and ℓ_w^+ and it is valid throughout both the full and intermediate roughness regimes. Rotta simply added a length Δz to the z-coordinate in the Van Driest model resulting in

$$\ell^+ = \kappa\,(z^+ + \Delta z^+)\left[1 - \exp\left(\frac{-(z^+ + \Delta z^+)}{\lambda_{v,s}^+}\right)\right] \tag{4.14}$$

where $\lambda_{v,s}^+$ is the value of λ_v^+ corresponding to smooth surfaces and is usually set equal to 26. Evaluating the above expression at $z^+ = 0$ provides a relation between ℓ_w^+ and Δz^+ such that

$$\ell_w^+ = \kappa \Delta z^+ \left[1 - \exp\left(\frac{-\Delta z^+}{\lambda_{v,s}^+}\right)\right] \tag{4.15}$$

There is no simple analytical solution to the integral of equation (4.6) when this model is used. Granville (1985) presents a convenient form of the equations for numerical integration. By equating the mixing length velocity profile, equation (4.6), to the logarithmic profile, equation (4.1), he obtains

$$B_1 = \int_0^{z^+} \frac{2}{1 + \sqrt{1 + (2\ell^+)^2}} dz^+ - \frac{1}{\kappa} log z^+ \tag{4.16}$$

Using the substitution

$$\log z^+ = \int_1^{z^+} \frac{dz^+}{z^+}$$

the integral of equation (4.16) can be broken into two terms so that

$$B_1 = \int_0^1 \frac{2}{1 + \sqrt{1 + (2\ell^+)^2}} dz^+ + \int_1^{z^+} \left[\frac{2}{1 + \sqrt{1 + (2\ell^+)^2}} - \frac{1}{\kappa z^+}\right] dz^+ \tag{4.17}$$

Granville claims that the integrand of the second integral goes to zero by $z^+ \approx 300$. Therefore, in evaluating B_1, it is not necessary to integrate all the way out to the actual z^+; which can be as high as 300,000 in our study. This allows much faster computational time as well as greater accuracy in evaluating the integral. It should be pointed out though that to obtain convergence of the second integral to 10^{-5}, we

found that z^+ must be at least 500 and in some cases as high as 4500. The required value of z^+ increased with the drag characterization function, B_1.

For large z^+, a fixed relation between B_1 and ℓ_w^+ can be generated using equation (4.17). This relation is shown in Figure 4.3 along with the analogous relation for the Rotta 1 model. Note that the Rotta 2 model predicts a non-zero wall mixing length in the intermediate roughness regime. Although this is considered objectionable by some, it is for this reason that we chose the Rotta 2 model. In the case of a boundary layer over the ocean, it seems quite probable that the wave motion will generate turbulence, and consequently a non-zero mixing length on the surface. Therefore, the Rotta 2 model seems to lend itself nicely, on a physical basis, to the problem at hand. It is based on a velocity profile which is non-logarithmic close to the surface and it provides a roughness parameter, (either Δz^+ or ℓ_w^+), which theoretically can be related to surface wave conditions.

4.3 Application of the Rotta 2 model

The Rotta 2 model relates $\overline{u}_{10}$, u_*, and Δz^+ or ℓ_w^+. The model can be applied in a number of ways but in each case we will specify $\overline{u}_{10}$ and either a stress estimate or a surface parameter while solving for the other. Note that B_1 varies with z^+ up to $z^+ \sim 5000$. This implies that the z^+ at which the model is applied must be outside this region so that the relation between B_1 and ℓ_w^+ holds. For our measurements at 10 m, the corresponding z^+ is always greater than 100,000 so that the relation between B_1 and ℓ_w^+ shown in Figure 4.3 will always hold.

The baseline test for the model was to use equation (3.9) to obtain a stress estimate for a given wind speed and then calculate the corresponding wall mixing length, ℓ_w^+. The mean wind speed, $\overline{u}_{10}$, and stress estimate, u_*, were used to obtain B_1 through equation (4.1). Then ℓ_w^+ was obtained from the relation shown in Figure 4.3. This test was done to insure that the model could produce the C_D regression line found for our

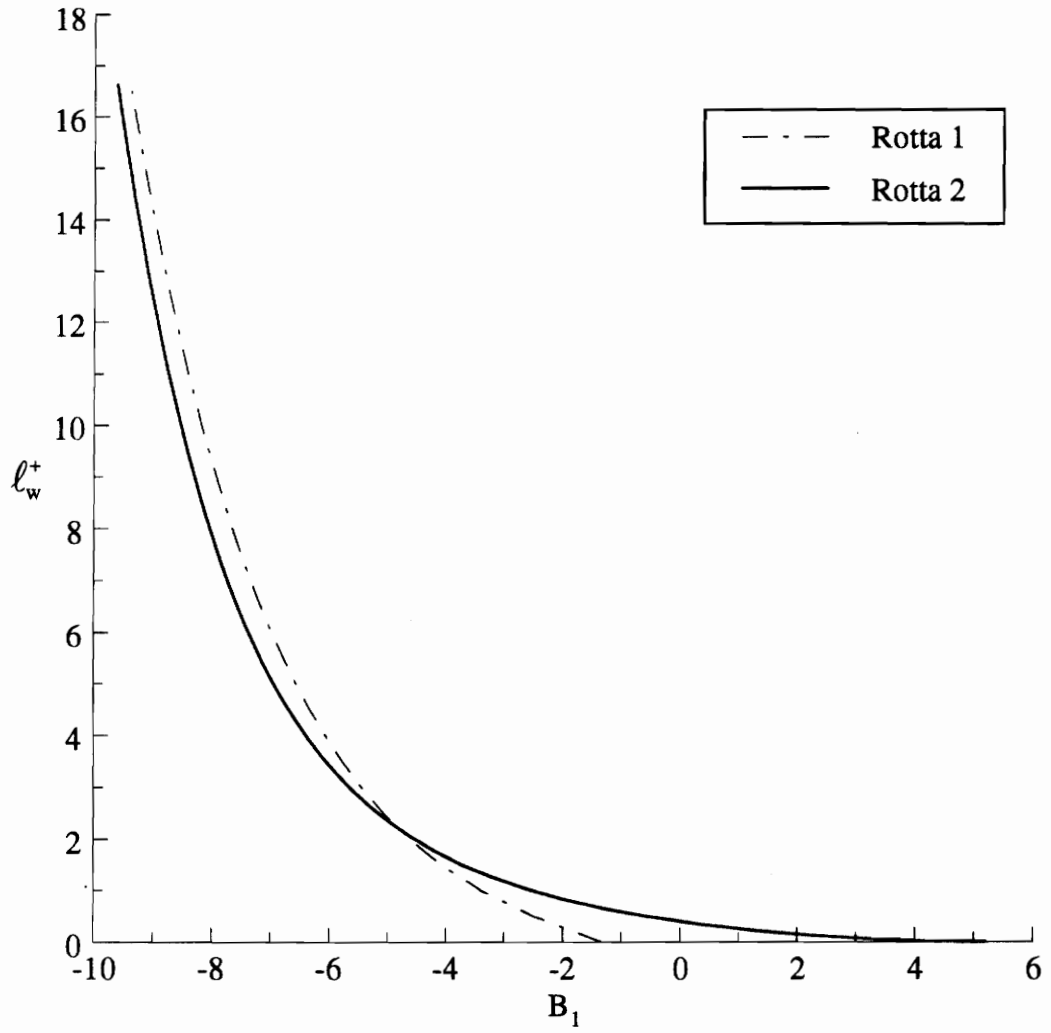

Figure 4.3: A comparison of the relation between the wall mixing length and the drag characterization function using the Rotta 1 and 2 models.

data. The resulting distribution of ℓ_w^+ with mean wind speed is shown in Figure 4.4 along with the Rotta 1 curve. This result is similar, in theory, to a single parameter wave spectrum; i.e. for a given wind speed, the model predicts the expected, (or average), surface conditions via the wall mixing length.

A more useful form of the model is to fix the wind speed and look at the variation in C_D as ℓ_w^+ changes. B_1 is fixed by the selection of ℓ_w^+ in the relation of Figure 4.3. Then u_* can be backed out of equation (4.1) and the resulting C_D is just $(u_*/\overline{u}_{10})^2$. A series of these curves are shown in Figure 4.5. All of the scatter within one of the intervals defined on Figure 3.5 lies along one of these curves. These curves are a first step in the development of a model which correlates the scatter in the drag coefficients to a wave surface parameter. However, the model can not be completed and actually tested until the fictitious surface parameter ℓ_w^+ is related to a physical surface wave parameter. As was mentioned earlier, this will have to wait for a future study when the wave data from this experiment has become available.

4.3.1 Velocity Profiles

For a given set of data, ($\overline{u}_{10}$, u_*, and ℓ_w^+), a velocity profile can be calculated from equation (4.6) where the distribution of ℓ^+ with z^+ is obtained from equation (4.14). (Note that if ℓ_w^+ is used, Δz^+ must first be calculated using equation (4.15)). $\overline{u}_{10}$ and u_* also fix the corresponding logarithmic velocity profile using equation (4.1).

Figure 4.6 displays a series of velocity profiles indicative of different roughness conditions. Note that the mixing length model gives one continuous profile valid throughout both the sublayer and logarithmic regions, which approaches the logarithmic profile, (the straight lines in Figure 4.6), at large z^+. For the smooth case the mixing length profile takes the familiar $u^+ = z^+$ form in the sublayer.

The departure from the logarithmic profile extends further from the surface as the roughness increases. For the smooth case, the mixing length profile becomes

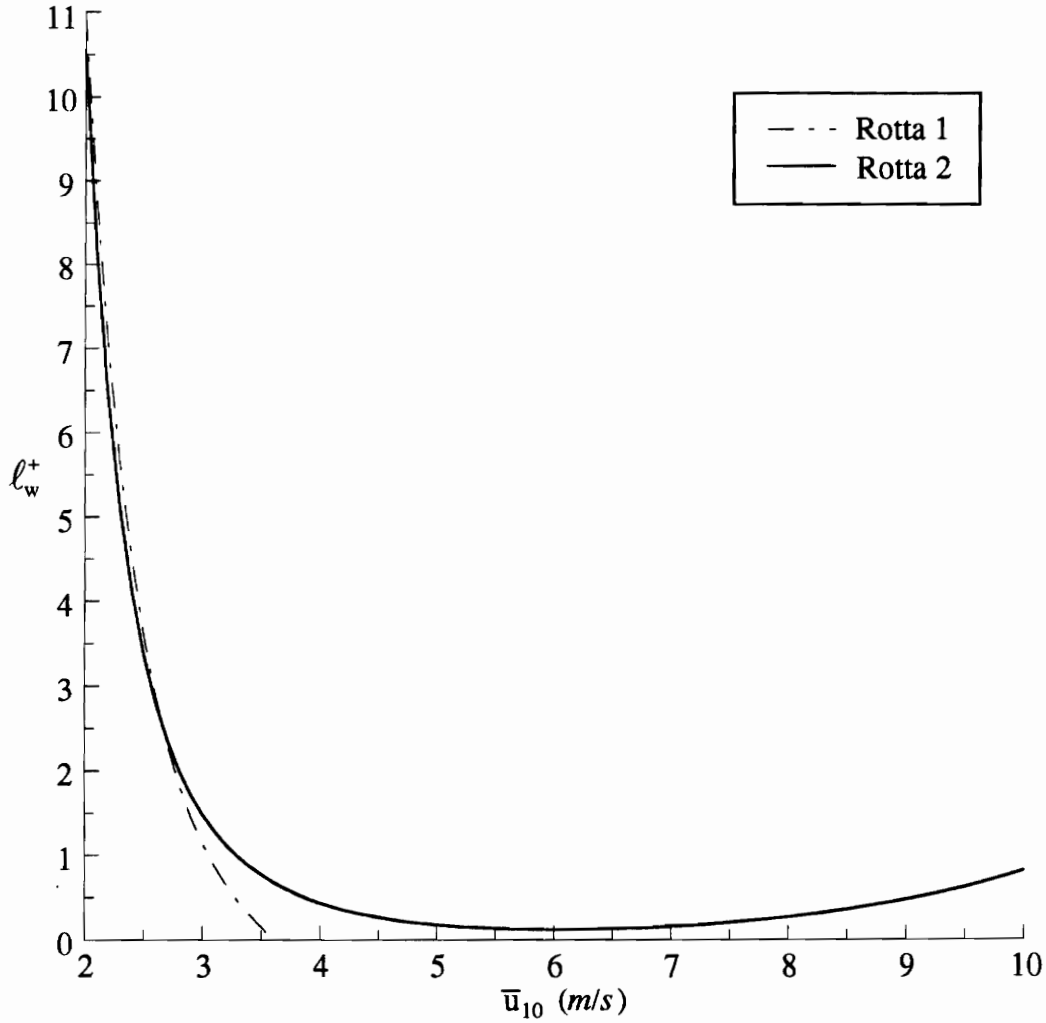

Figure 4.4: Expected wall mixing length for a given mean wind speed using the Rotta 1 and 2 models and the C_D regression line for our data.

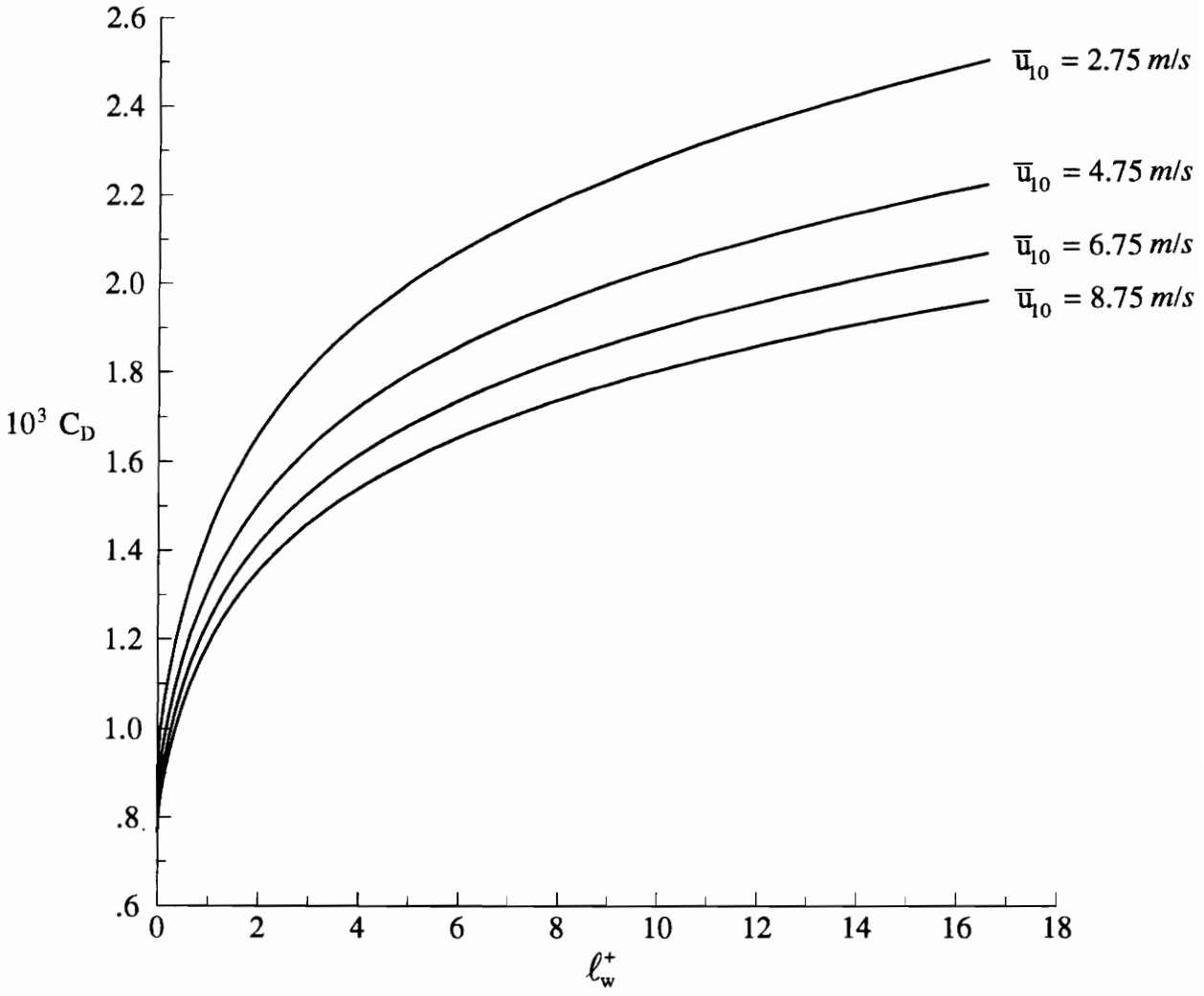

Figure 4.5: Curves of constant mean wind speed depicting the dependence of the drag coefficient on the wall mixing length using the Rotta 2 model.

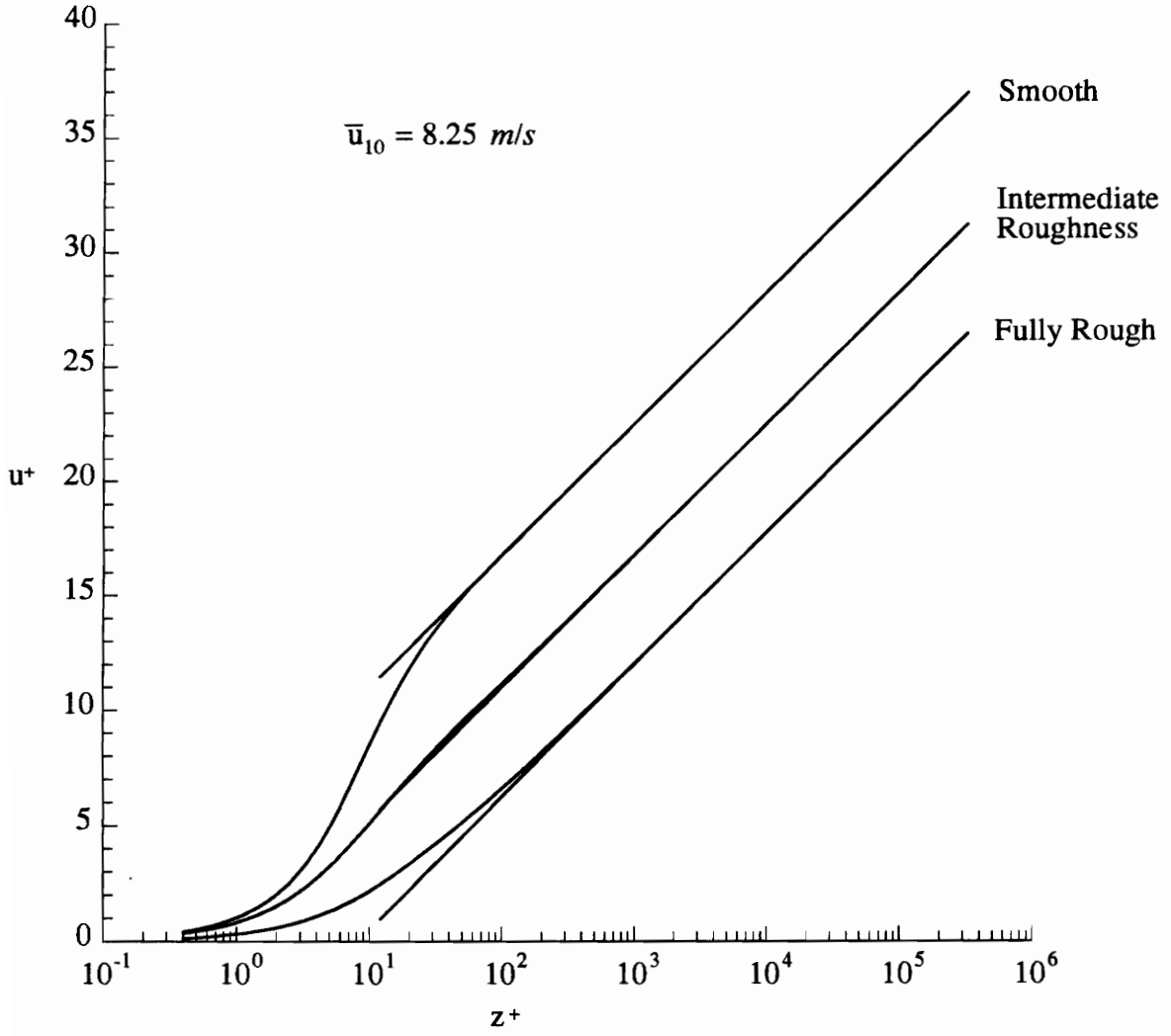

Figure 4.6: Velocity profiles obtained using the Rotta 2 model. Logarithmic profiles are shown in the outer region.

logarithmic by $z^+ = 50$ indicating essentially no departure as is expected. The point at which each case becomes logarithmic is really already known from the calculation of B_1 in equation (4.17). The point at which the second integral in equation (4.17) converges is the point at which the profile becomes logarithmic because we know that for a logarithmic profile, B_1 is a constant.

Chapter 5

Conclusions and Future Work

The modified eddy correlation technique presented here has been successfully applied to the data set obtained during the Bight of Abaco experiments. The technique allows for the calculation of accurate stress estimates from relatively simple, low frequency data acquisition systems. The resulting C_D's displayed similar trends to previous studies of the moderate wind speed range. Our data also supports the concept of a rise in drag coefficient at low wind speeds which has been identified by at least one previous investigator, (i.e. Geernaert et al. 1988). The large amount of data obtained for a given wind speed or direction should allow for future studies into the dependence of the drag coefficient on things other than the mean wind.

The calculation of drag coefficients for the 1991 data must still be completed. This data will further expand the already huge data set for the Bight of Abaco as well as provide a means of testing some of the assumptions made in processing the 1990 data. The resulting stability corrected C_D regression line can be compared to the 1990 curve presented here. If our assumption about the stability conditions during the 1990 experiment is correct, these two curves should be very similar. Also, more data from the same region will help in investigating the alignment of the wind stress vector with the mean wind.

The second phase of this study resulted in the use of a mixing length model to describe the scatter in the C_D plots due to varying surface conditions. The selection of Rotta's second model for l^+ was based on its unique ability to predict a velocity profile with a departure from logarithmic close to the surface and a non-zero wall mixing length in both the fully rough and intermediate roughness regimes. The usefulness of this model will depend on the success of relating the wall mixing length described here to a more physical surface wave parameter.

As with any flow model, especially in the boundary layer region, the validity of the model presented here is difficult to prove. Assuming again that a connection can be made between the wall mixing length and surface conditions, a first step in proving or disproving this model would be to compare the predicted surface conditions with those actually observed in the bight. This information will be readily available to us because for each data record of turbulent wind information, there is wave data taken from the same region. This wave data is still being processed and should become available in the Spring of 1993.

Another method for testing the model presented here would be to design an experiment in which the velocity profile could be measured directly while at the same time measure the turbulent wind fluctuations. In this way the predicted departure from the logarithmic profile could be checked. Unfortunately, for the scaling variables currently used, the departure from logarithmic turns out to be within 1 cm of the surface. However, it is proposed that the kinematic viscosity, ν, currently used to non-dimensionalize z may be inappropriate for the large scale motions of the atmosphere. A more suitable scaling parameter may be the fictitious eddy viscosity which can be related to the wall mixing length. This appears to move the departure out to around 0.5 m which is in accordance with the observations of Takeda (1963). A further investigation into this concept is required.

REFERENCES

[1] Balachandran, B., Energy Transfer from Wind to Waves, M.S. thesis, Virginia Polytechnic Institute and State Univeristy, 1986.

[2] Donelan, M.A., The dependence of the aerodynamic drag coefficient on wave parameters, in the First International Conference on Meteorology and Air-Sea Interaction of the Coastal Zone, *Amer. Met. Soc.*, Boston, 381–387, 1982.

[3] Fairall, C.W. and S.E. Larsen, Inertial-dissipation methods and turbulent fluxes at the air-ocean interface, *Bound. Layer Met.*, 34, 287–301, 1986.

[4] Geernaert, G.L., Drag coefficient modelling for the near-coastal zone, *Dyn. Atmos. Oceans*, 11, 307–322, 1988a.

[5] Geernaert, G.L., K.L. Davidson, S.E. Larsen, and T. Mikkelsen, Wind stress measurements during the Tower Ocean Wave and Radar Dependence experiment, *J. Geophys. Res.*, 93, 13,913–13,923, 1988b.

[6] Geernaert, G.L., Bulk parameterizations for the wind stress and heat flux, in *Surface Waves and Fluxes: Theory and Remote Sensing*, vol. 1, edited by G. Geernaert and W. Plant, Kluwer Academic, Boston, Mass., 1990.

[7] Granville, P.S., Mixing-length formulations for turbulent boundary layers over arbitrarily rough surfaces, *J. Ship Res.*, 29, No. 4, 223–233, 1985.

[8] Hsu, S.A., A dynamic roughness equation and its application to wind stress determination at the air-sea interface, *J. Phys. Oceanogr.*, 4, 116–120, 1974.

[9] Large, W.G., The turbulent fluxes of momentum and sensible heat over the open ocean during moderate to strong winds, Ph.D. dissertation, Univ. of British Colombia, Vancouver, B.C., 1979.

[10] Large, W.G., and S. Pond, Open ocean momentum flux measurements in moderate to strong winds, *J. Phys. Oceanogr.*, 11, 324–336, 1981.

[11] Marple, S.L., Jr. *Digital Spectral Analysis with Applications*, Prentice–Hall, Englewood Cliffs, N. J., 1987.

[12] Panofsky, H.A. and Dutton, J.A. *Atmospheric Turbulence - Models and Methods for Engineering Applications*. John Wiley & Sons, Inc., 1984.

[13] Prandtl, L., Über die ausgebildete turbulenz, *Z. Angew. Math. Mech.*, 5, 136–139, 1925.

[14] Rotta, J., Das in wandnähe gültige geschwindigkeitsgesetz turbulenter strömungen, *Ingenieur-Archiv*, 18, 277–280, 1950

[15] Rotta, J., Turbulent boundary layers in incompressible flow, *Progress in Aeronautical Sciences*, A. Ferri, D. Küchemann, and L. H. G. Sterne, editors, Pergamon Press, New York, vol. 2, 1–219, 1962.

[16] Snyder, R.L., Neu, W.L., Long, R.B., De Voogt, W.J.P., A Long Range Program to Parameterize the Two-Dimensional Evolution of the Surface Gravity Wave Field. *Nova Univ. Oceanographic Center Technical Report.*, 1990.

[17] Takeda, A., Wind profiles over sea waves, *J. Oceanogr. Soc. of Japan*, 19, no. 3, 16–22, 1963

[18] van Driest, E.R., On turbulent flow near a wall, *J. Aero. Sci.*, 23, 1007–1011, 1956

[19] Wei, C., Evolution of the dynamic characteristics of the K-Gill anemometer, M.S. thesis, Virginia Polytechnic Institute and State University, 1990.

VITA

The author was born in Acton, Massachusetts on May 22, 1969. He entered the Aerospace and Ocean Engineering program at Virginia Polytechnic Institute and State University in 1987. He received his Bachelor of Science degree, Cum Laude, in December of 1991. He began the research leading to this thesis in May, 1991 and officially entered the Master's program in January, 1992.